RESEARCH ARTICLE | APRIL 02 2025

Revisiting the laminar plume

Alan Shapiro ; Jeremy A. Gibbs

Physics of Fluids 37, 043604 (2025)
https://doi.org/10.1063/5.0260318

Physics of Fluids ARTICLE pubs.aip.org/aip/pof

Revisiting the laminar plume

Cite as: Phys. Fluids **37**, 043604 (2025); doi: 10.1063/5.0260318
Submitted: 23 January 2025 · Accepted: 11 March 2025 ·
Published Online: 2 April 2025

Alan Shapiro[1,a] and Jeremy A. Gibbs[2]

AFFILIATIONS

[1]School of Meteorology, University of Oklahoma, Norman, Oklahoma 73072, USA
[2]NOAA/OAR National Severe Storms Laboratory, Norman, Oklahoma 73072, USA

[a]Author to whom correspondence should be addressed: ashapiro@ou.edu

ABSTRACT

We revisit the classical problem of a laminar plume arising from a point source of heat on a horizontal boundary of infinite extent in an otherwise motionless neutrally stratified environment. The Boussinesq equations of motion and thermal energy for a steady axisymmetric plume are approximated separately for the plume interior and exterior, with the two regions connected via pressure continuity and use of the transverse (radial) equation of motion, an equation that has not been used in previous theoretical analyses of laminar plumes. An analysis of the governing equations yields a simple relation between the azimuthal vorticity and buoyancy, two variables of prime interest in studies of axisymmetric thermals, plumes, and jets. The relation states that when the Prandtl number is 1, the vorticity is equal to the buoyancy times radius divided by twice the kinematic viscosity. A more complex vorticity–buoyancy relation is obtained for arbitrary Prandtl numbers. The same vorticity–buoyancy relations are predicted for the plume interior and exterior. The relation for a Prandtl number of 1 is validated using output from a direct numerical simulation of a laminar plume induced by a small heat source on the lower boundary. The steady-state vorticity–buoyancy relation is confirmed in regions that have attained a steady state and also, remarkably, at earlier times, where the plume cap has passed, but the flow is still evolving.

I. INTRODUCTION

Thermally induced plumes are common in a variety of geophysical and engineering contexts. Plumes of hot air heated by the ground during the afternoon rise through the atmospheric boundary layer.[1–4] Plumes of superheated mantle material rise above thermal anomalies on the Earth's core/mantle interface.[5–8] Plumes are important to the ventilation and heating of buildings, the cooling of electronic circuitry, and the heat transfer in heat exchangers.[9–12] Although many plumes are turbulent, turbulent plumes can arise from laminar plumes that have become unstable at certain distances above their sources (e.g., smoke from a cigarette). The laminar plume is of interest in its own right as a canonical natural convective flow[13–15] and can also be used as a base state in studies of flow transitions and pathways to turbulence.

In this study, we revisit the laminar plume arising from a maintained point source of heat in a neutrally stratified environment otherwise at rest. Laboratory experiments[6,16–29] show that laminar plumes consist of a rising cap (also known as a front or head) of buoyant fluid on top of a narrow stem (also known as a column, corridor, or conduit) of buoyant fluid that extends from the heat source up to the base of the cap. Although the caps are often mushroom-shaped, other morphologies are possible.[21,26] As the cap ascent speed is less than the vertical velocity of the fluid flowing through the stem, the cap is continually fed by its stem, and its volume increases. In contrast, flow within the stem rapidly approaches a steady state.

Theoretical results for the structure of a steady laminar plume over a maintained point source of heat were first obtained by Zeldovich[30] (English translation in Ostriker *et al.*[31]). Zeldovich[30] showed that the simplified governing equations (essentially Boussinesq-approximated equations with additional approximations based on the slenderness of the plume) admitted solutions for the buoyancy and vertical velocity fields as products of powers of z and functions of the similarity variable $\xi \propto r/z^{1/2}$ [z is the height and r is the distance from the plume axis (radius)]. The power laws predicted (i) a z-independent centerline ascent speed, (ii) a centerline buoyancy that decreased as $1/z$, and (iii) a plume width that increased as $z^{1/2}$ (the latter result was not given explicitly, but could be inferred from the presented results, and was clearly used in a Reynolds number calculation). The explicit forms of the similarity functions were not pursued. The power laws are summarized in the Appendix.

Independently, Yih[32] considered the same laminar axisymmetric problem as in Zeldovich,[30] obtained the same power laws and derived analytical solutions of the coupled ordinary differential equations for the similarity functions for Prandtl numbers (Pr) 1 and 2

(although Yih,[14] p. 411, noted that there are some numerical errors in Yih[32]).

Fujii[33] and Brand and Lahey[34] rediscovered the Yih[32] solutions for Pr = 1 and 2 and also integrated the similarity model equations numerically for other Pr. For the Pr = 1 and 2 cases, the similarity solution for the vertical velocity was proportional to $1/(1 + a\xi^2)^2$, where ξ is the same similarity variable as in Zeldovich[30] (in different notation), and a is a constant (different for the two Pr cases). Thus, at any height, the vertical velocity decreased monotonically with r and approached 0 as $r \to \infty$.

The similarity models described above were designed for the plume interior, where it was assumed that the vertical acceleration, buoyancy, and radial diffusion of vertical velocity were of the same order of magnitude and that the vertical parts of the divergence of the viscous/diffusive heat and momentum fluxes were negligible. The similarity form of the temperature field was validated in laboratory experiments by Shlien and Boxman[18,19] and Davaille *et al.*[27] The velocity field was validated by Tanny and Shlien.[20] Good agreements between predictions from the similarity theory and observations were obtained when a virtual source correction was used to take into account the small (but non-zero) size of the heaters.

The purpose of this study is to show how a fundamental relation exists between the azimuthal vorticity and buoyancy, two variables of prime interest in studies of axisymmetric thermals, plumes, and jets. As part of the derivation of this relation, separate approximations and analyses are made for the plume interior and plume exterior, a partition analogous to the Prandtl partition of flow over a flat plate into boundary-layer and external regions.[35] The same vorticity–buoyancy relation is found to apply to the plume interior and exterior. As part of the derivation, the radial equation of motion—which was not used in the development of the similarity models—is integrated with respect to radius, and pressure continuity is imposed at the interface between the plume interior and exterior. The vorticity-buoyancy relation is remarkably simple for Pr = 1, but a related (more complex) relation is found for arbitrary Pr. To motivate some of the assumptions used in our derivation and provide a dataset to test our prediction, we performed a direct numerical simulation (DNS) of a laminar axisymmetric plume for Pr = 1.

A summary of the DNS, including comparisons with the similarity theory and laboratory experiments, is provided in Sec. II. In Sec. III, the governing equations are approximated for the plume interior and exterior, and partially integrated, with the same differential relation between buoyancy and azimuthal vorticity obtained for both regions. Integration of this relation in Sec. IV yields a simple formula for vorticity in terms of buoyancy when Pr = 1 and a more complex relation for arbitrary Pr. The predicted relation for Pr = 1 is found to be in excellent agreement with the corresponding DNS relation in both the plume interior and exterior after the steady state has been reached and also, remarkably, at times after cap passage but before the flow has attained a steady state. We attempt to make this latter result plausible in Sec. V by retracing the derivations in Sec. III using unsteady versions of the governing equations.

II. DIRECT NUMERICAL SIMULATION

A. Numerical model

We conducted a direct numerical simulation (DNS) of a laminar axisymmetric plume using the open-source computational fluid dynamics code MicroHH of van Heerwaarden *et al.*[36] The numerical mesh consisted of 2048 × 2048 × 2048 points in the Cartesian x, y, and z directions (z is height) with a uniform grid spacing $\Delta = 0.002$ m, giving a computational domain of dimensions $4.096 \times 4.096 \times 4.096\ \mathrm{m}^3$. The governing equations were the Boussinesq-approximated equations of motion, thermal energy, and mass conservation (incompressibility condition). The equations of motion and thermal energy were spatially discretized on a staggered Arakawa C-grid and integrated with second-order finite differencing of the advection and diffusion terms. The perturbation pressure was solved using a second-order Poisson solver. The model was integrated with a third-order Runge-Kutta scheme using adaptive time stepping. The kinematic viscosity ν and thermal diffusivity κ were set to $10^{-5}\ \mathrm{m}^2\ \mathrm{s}^{-1}$ (Pr = 1). The initial velocity and buoyancy profiles were set to zero, and the environment was neutrally stratified. The vertical velocity w was set to zero on the lower and upper boundaries. The x-velocity component u and y-velocity component v satisfied the no-slip condition on the lower boundary and the free-slip (zero normal gradient) condition on the upper boundary. A zero-normal-gradient condition was applied to the buoyancy at the upper boundary, while on the lower boundary the buoyancy was set to $0.125\ \mathrm{m\ s}^{-2}$ on a small block of the four central-most grid points and zero elsewhere. The lateral boundary conditions for all prognostic fields were periodic.

B. Plume simulation

The DNS was run until the cap and upper part of the stem became unstable, about 30 s into the simulation. An overview of the plume rise is shown in Fig. 1. The leading edge of the cap rises at a nearly constant rate ($\approx 0.09\ \mathrm{m\ s}^{-1}$), especially from time $t = 10$ to 25 s. Constant cap speeds have been described in laboratory experiments on laminar plumes by Shlien,[16,17] Moses *et al.*,[22] Moses *et al.*,[23] Kaminski and Jaupart,[24] Davaille *et al.*,[27] Cagney *et al.*,[28] and others, though for Prandtl numbers 1–5 orders of magnitude larger than in our DNS. The notable increase in the width and depth of the cap with time is consistent with cap growth through a continual supply of warm fluid rising through the stem at a faster rate than the ascent speed of the cap.

A vertical cross section of the streamlines at $t = 20$ s (Fig. 2) depicts upward and outward displacements of environmental fluid in advance of the rising cap and the entrainment of environmental fluid into the stem. The flow exterior to the plume becomes increasingly horizontal as the ground is approached. Figure 2 also shows that the plume is surrounded by subsiding fluid ($w < 0$). As the similarity solution for w discussed in Sec. I is positive everywhere (it attains its peak on the plume axis, decreases monotonically with r, and approaches 0 as $r \to \infty$), it cannot apply to this exterior region.

Three measures of plume radius $R(z)$ are shown in Fig. 3 at $t = 25$ s. The R are defined by radii where (i) $\partial^2 w/\partial r^2 = 0$ (w inflection point; approximate location of peak azimuthal vorticity), (ii) $w = 0$ (interface between plume updraft and downdraft), and (iii) $\partial w/\partial r = 0$ (peak downdraft). The inflection point yields the smallest R, and the peak downdraft yields the largest. The curves of R vs z are piecewise constant because our calculations using the DNS data restricted R to multiples of the grid spacing. The radii defined by the $w = 0$ and $\partial w/\partial r = 0$ curves were checked against power law (A3) [$R = C z^{1/2}$] using visual estimates of R from Fig. 3. The inflection point curve was not checked because its piecewise nature made its assessment particularly difficult. The $w = 0$ and $\partial w/\partial r = 0$ curves at $z = 0.1$ m yielded

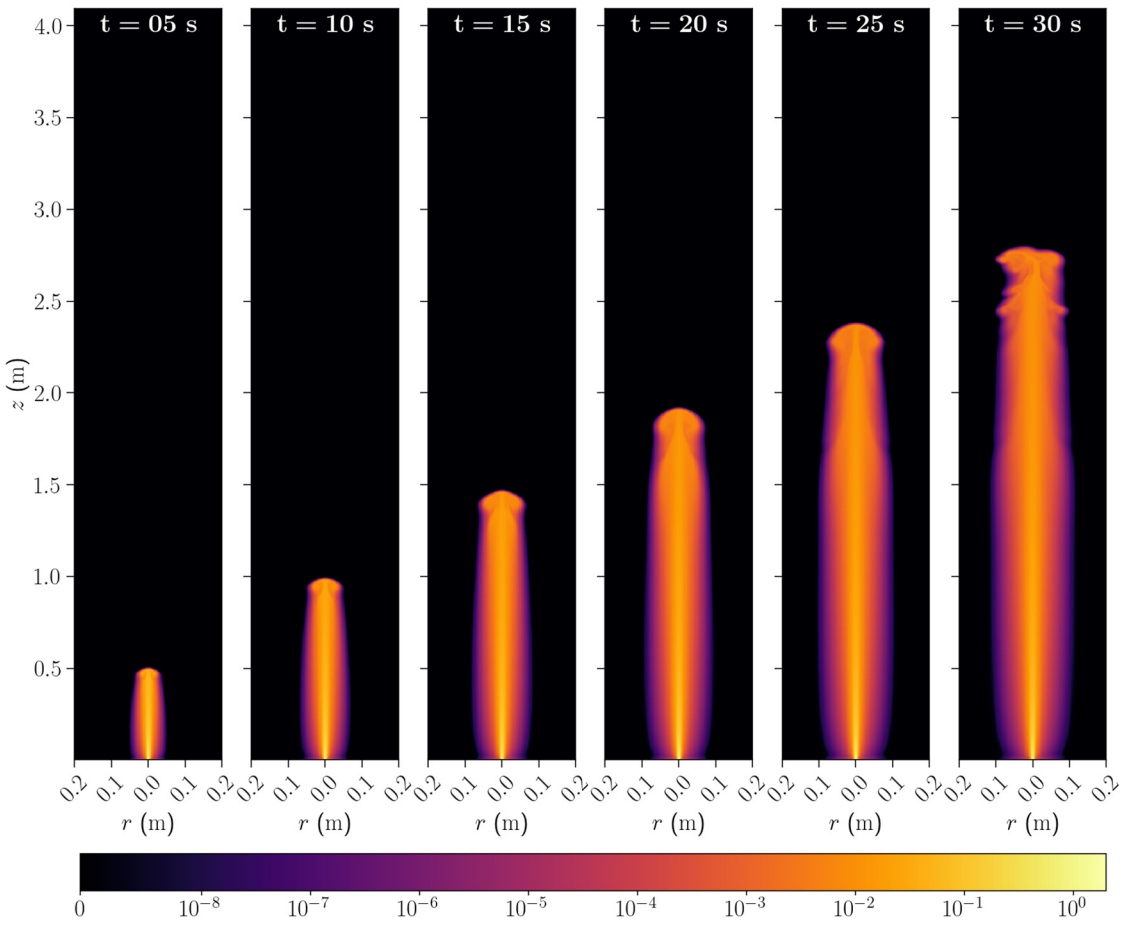

FIG. 1. Vertical cross section of buoyancy (m s^{-2}) at 5 s intervals. Only a portion of the 4 m wide computational domain is displayed.

$R = 0.045$ and 0.065 m, respectively. These were used to obtain $C = R/(0.1\,\mathrm{m})^{1/2} = 0.142\,\mathrm{m}^{1/2}$ and $0.206\,\mathrm{m}^{1/2}$, respectively, from which we calculated the R at $z = 0.2$ m as $R = C\,(0.2\,\mathrm{m})^{1/2} = 0.064$ and 0.092 m. Subtracting these latter values from the corresponding R observed at $z = 0.2$ m (0.059 and 0.081 m) and normalizing the differences by the latter observed values, yielded 8.5% and 13.6% discrepancies between the $w = 0$ and $\partial w/\partial r = 0$ curves and the power law. In our study, it will be convenient to work with R defined as the radius at which $w = 0$,

$$w|_{r=R} = 0. \tag{1}$$

The radial dependences of the buoyancy b and velocity components at $t = 25$ s at selected low-altitudes in the plume interior are shown in Fig. 4. On each level, the peak w is ~100 times larger than the peak u (~indicates "on the order of magnitude of"), though there is a trend for the ratio of peak w to peak u to decrease with height. Consistent with power laws (A1) and (A2), Fig. 4 shows that w along the centerline ($r = 0$) is nearly independent of z, while the centerline buoyancy varies approximately as z^{-1} ($z^{-0.96}$ based on data at $z = 0.1$ and 1.0 m; $z^{-1.00}$ based on data at $z = 0.1$ and 0.25 m). Consistent with power law (A9), which yields $\partial u/\partial z > 0$ ($C > 0$, $F > 0$, $G > 0$, $\partial G/\partial r < 0$), Fig. 4 shows that $u < 0$ (inflow) with a magnitude that decreases with height, so $\partial u/\partial z > 0$. Additional plots of u (not shown) suggest that the boundary layer along the no-slip lower boundary is about 3 cm deep in the vicinity of the plume.

The buoyancy and velocity components for the same time and heights as in Fig. 4 are shown in Fig. 5 for the plume exterior. As in the plume interior, $u < 0$ with a magnitude that decreases with height ($\partial u/\partial z > 0$). There is descent ($w < 0$) throughout the exterior (as noted, this descent indicates the inapplicability of the similarity model in this region), with the peak downdraft located just outside the plume edge. The peak w is ~100 times smaller than the peak u.

The azimuthal vorticity,

$$\eta \equiv \frac{\partial u}{\partial z} - \frac{\partial w}{\partial r}, \tag{2}$$

and $\partial u/\partial z$ $\partial w/\partial r$ individually are shown in Fig. 6 at $t = 25$ s at height $z = 0.25$ m. In the plume interior, $\eta \approx -\partial w/\partial r$. In contrast, in the plume exterior, where $\partial u/\partial z$ and $-\partial w/\partial r$ are nearly equal and opposite, $\partial u/\partial z - \partial w/\partial r \approx 0$, and the flow is nearly irrotational, as in the previous studies (e.g., Taylor,[37] Kraemer,[38] and Moses *et al.*[22]). A simple expression for u in this region is the equation for

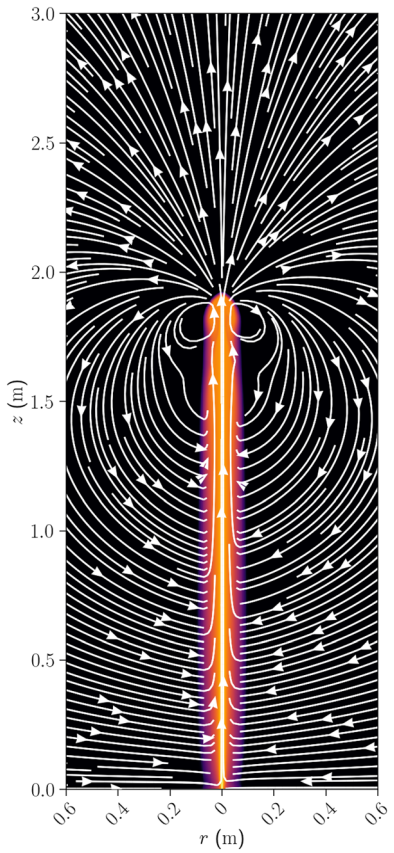

FIG. 2. Vertical cross section of buoyancy and streamlines at $t = 20$ s (corresponding to fourth panel of Fig. 1).

irrotational flow into an axial line sink, $u = UR/r$, where $U \equiv u|_{r=R}$. As seen in Fig. 5(a), this sink solution is an excellent approximation to u from the DNS.

The evolution of w and b in the plume interior at $z = 0.25$ m is shown in Fig. 7. At $t = 1$ and 2 s, the cap has not yet crossed the $z = 0.25$ m level and the ascent results from the near-irrotational pushing of fluid away from the advancing cap. At those times, b is essentially zero (values less than 10^{-6} m s^{-2} do not appear on the diagram) which is consistent with the fact that vertical motion in a neutrally-stratified environment cannot change the fluid buoyancy. At later times, the curves of both w and b saturate, with a "point of steadiness" spreading radially outward from the plume axis. Since the flow at the largest displayed radius $r = 0.06$ m at the later times is still evolving, so are the $w = 0$ and $\partial w/\partial r = 0$ curves in Fig. 3, at least at (and presumably above) $z = 0.25$ m.

Figure 8 shows the evolution of w along the plume axis at various heights. This centerline w is nearly 0 m s^{-1} from $t = 0$ s until cap passage, when it increases explosively and then rapidly overshoots and undershoots its steady-state value. Cap passage is rapid, taking place within 1 s on the $z = 0.25$ m level. The steady state centerline updraft speed of ≈ 0.19 m s^{-1}, which is largely independent of z [consistent with Eq. (A1)], is slightly more than twice the cap speed. The evolution of the sum $S \equiv \sum r\,b\,w$ over all points in a line from the plume axis to the edge of the computational domain (S is proportional to the buoyancy flux F) depicted in Fig. 9 is similar to that of w along the plume axis.

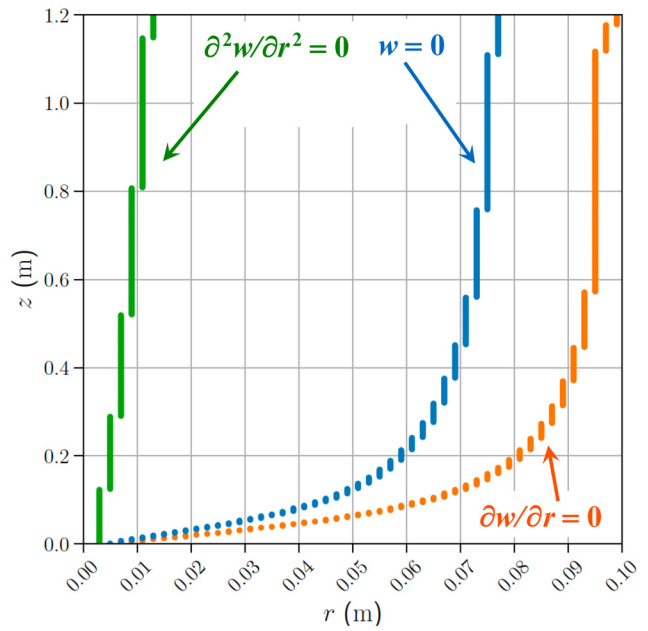

FIG. 3. Height dependences of three measures of plume radius $R(z)$ at $t = 25$ s: radius where (i) $\partial^2 w/\partial r^2 = 0$, (ii) $w = 0$, and (iii) $\partial w/\partial r = 0$. The R used in our derivations is the radius where $w = 0$.

III. THEORETICAL ANALYSIS OF THE STEADY STATE

A. Governing equations prior to approximations in the plume interior and exterior

We analyze the laminar axisymmetric plume theoretically, in its steady state, using a cylindrical polar coordinate system with origin at the heat source and axial coordinate pointing vertically; r is the radial coordinate, z is the vertical (axial) coordinate (ground at $z = 0$), u is the radial velocity component ($u < 0$ indicates inflow), and w is the vertical velocity component. The dependent variables are independent of the azimuthal coordinate, and there is no azimuthal velocity component. The motion is governed by the steady Boussinesq-approximated radial and vertical equations of motion,

$$u\frac{\partial u}{\partial r} + w\frac{\partial u}{\partial z} = -\frac{\partial \Pi}{\partial r} + \nu\left[\frac{1}{r}\frac{\partial}{\partial r}\left(r\frac{\partial u}{\partial r}\right) + \frac{\partial^2 u}{\partial z^2} - \frac{u}{r^2}\right], \quad (3)$$

$$u\frac{\partial w}{\partial r} + w\frac{\partial w}{\partial z} = -\frac{\partial \Pi}{\partial z} + b + \nu\left[\frac{1}{r}\frac{\partial}{\partial r}\left(r\frac{\partial w}{\partial r}\right) + \frac{\partial^2 w}{\partial z^2}\right], \quad (4)$$

the thermal energy equation,

$$\frac{1}{r}\frac{\partial}{\partial r}(rub) + \frac{1}{r}\frac{\partial}{\partial z}(rwb) = \frac{\nu}{\mathrm{Pr}}\left[\frac{1}{r}\frac{\partial}{\partial r}\left(r\frac{\partial b}{\partial r}\right) + \frac{\partial^2 b}{\partial z^2}\right], \quad (5)$$

and the Boussinesq form of mass conservation equation (incompressibility condition),

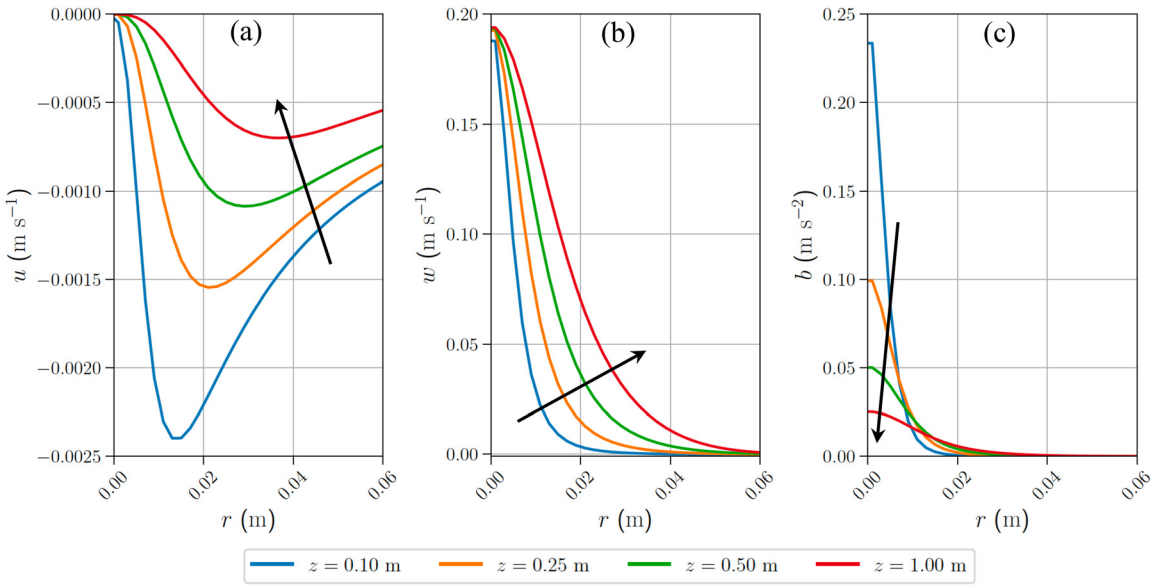

FIG. 4. Radial profiles of (a) u, (b) w, and (c) b in the plume interior at $t = 25$ s at selected heights. Arrows point toward increasing z.

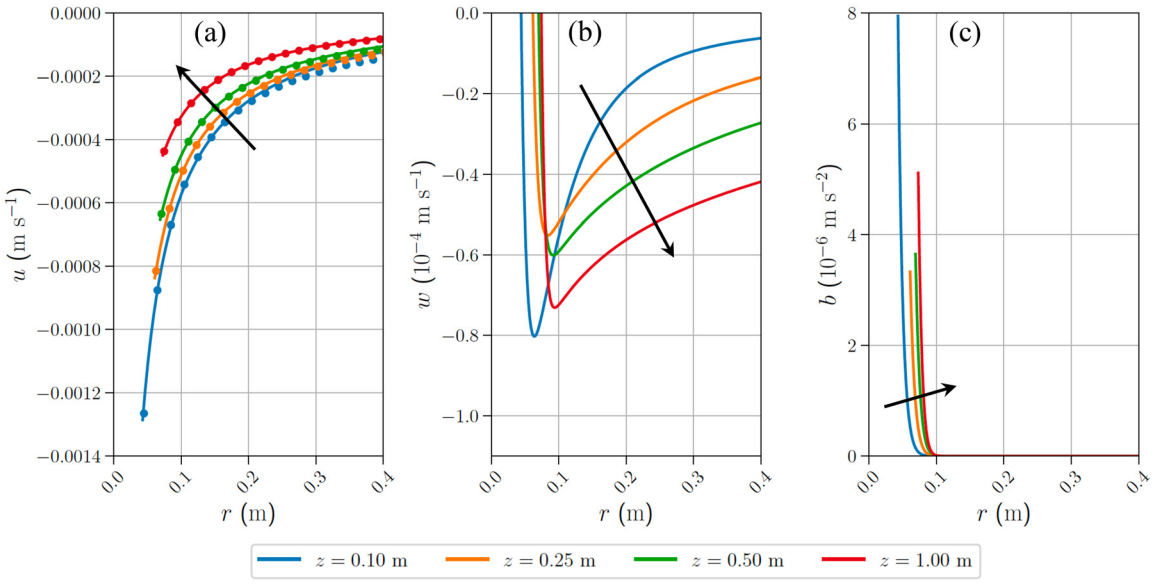

FIG. 5. As in Fig. 4, but for the plume exterior. The dots on the u-panel represent the approximate solution $u = UR/r$, where $U \equiv u|_{r=R}$.

$$\frac{\partial u}{\partial r} + \frac{u}{r} + \frac{\partial w}{\partial z} = 0. \tag{6}$$

Here, $\Pi \equiv (P - P_r)/\rho_{r0}$ is the kinematic perturbation pressure [P is the pressure, $P_r = P_r(z)$ is the pressure in a motionless reference environment, and ρ_{r0} is a constant reference value of density] and $b \equiv g(\Theta - \Theta_r)/\Theta_{r0}$ is the buoyancy [Θ is the potential temperature, $\Theta_r = \Theta_r(z)$ is the potential temperature in the reference environment, $\Theta_{r0} \equiv \Theta_r(0)$, g is the acceleration due to gravity]. The Prandtl number $\mathrm{Pr} \equiv \nu/\kappa$ is constant, as are ν and κ. To facilitate integration of the governing equations, we have put the advection terms in Eqs. (3) and (4) in the advective form, but the advection terms in Eq. (5) in the flux form.

The governing equations will be approximated separately in the plume exterior ($r > R$) and interior ($0 < r < R$) and integrated with respect to r. The integrated equations will be evaluated using the centerline conditions

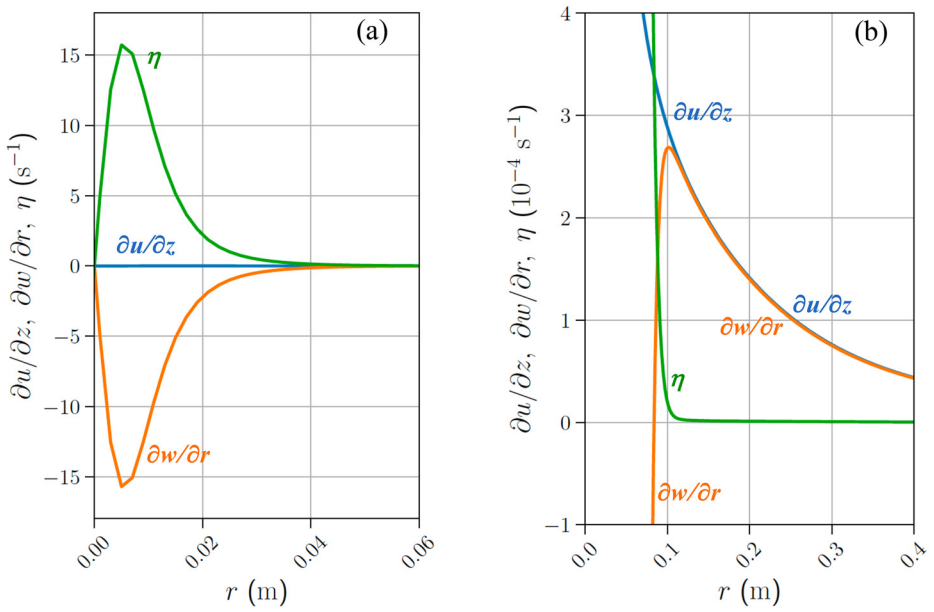

FIG. 6. Radial profiles of $\partial u/\partial z$, $\partial w/\partial r$, and $\eta \equiv \partial u/\partial z - \partial w/\partial r$ at $t = 25$ s at height $z = 0.25$ m in (a) plume interior and (b) plume exterior.

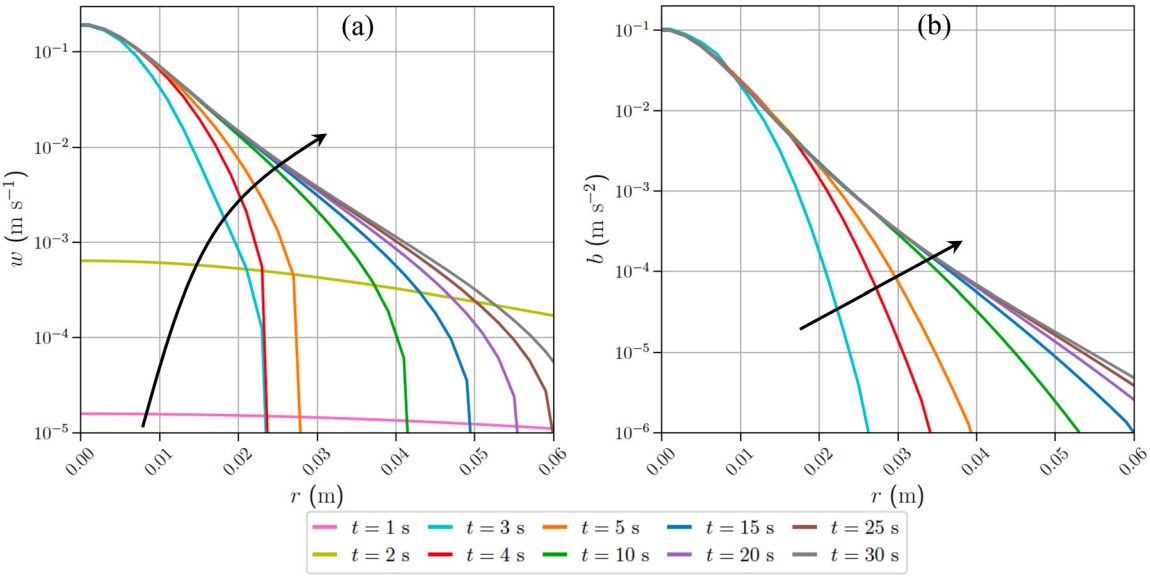

FIG. 7. Radial profiles of (a) w and (b) b at selected times at height $z = 0.25$ m in the plume interior. Results are shown at 1 s intervals for $t < 5$ s and at 5 s intervals for $t > 5$ s. Arrows point toward increasing t.

$$u|_{r=0} = 0, \quad \left.\frac{\partial w}{\partial r}\right|_{r=0} = 0, \quad \left.\frac{\partial b}{\partial r}\right|_{r=0} = 0, \tag{7}$$

(so $\eta|_{r=0} = 0$), the remote ($r \to \infty$) conditions

$$\lim_{r\to\infty} u = 0, \quad \lim_{r\to\infty} b = 0, \quad \lim_{r\to\infty} \Pi = 0, \tag{8}$$

and continuity of Π across the plume edge, with R defined through Eq. (1).

B. Steady plume exterior

Motivated by the DNS results, we consider flow in the exterior region at low altitudes but above the ground-based boundary layer. For scaling purposes, we consider this flow to be nearly irrotational ($\partial u/\partial z \sim \partial w/\partial r$) and mostly horizontal ($u \gg w$, which is shorthand for $|u| \gg |w|$). These relations scale as $\mathscr{U}^E/\mathscr{H}^E \sim \mathscr{W}^E/\mathscr{L}^E$ and $\mathscr{U}^E \gg \mathscr{W}^E$, where $\mathscr{U}^E$ and $\mathscr{W}^E$ are the radial and vertical velocity scales, and $\mathscr{L}^E$ and $\mathscr{H}^E$ are the radial and vertical length scales

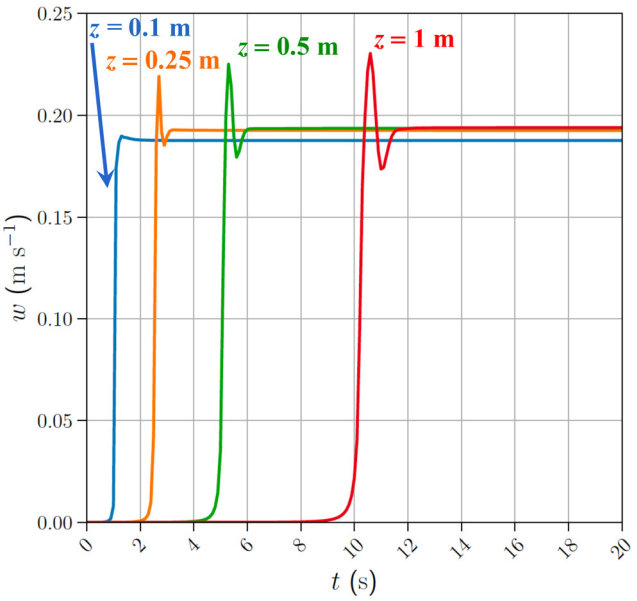

FIG. 8. Evolution of w on the plume axis ($r = 0$) at selected heights.

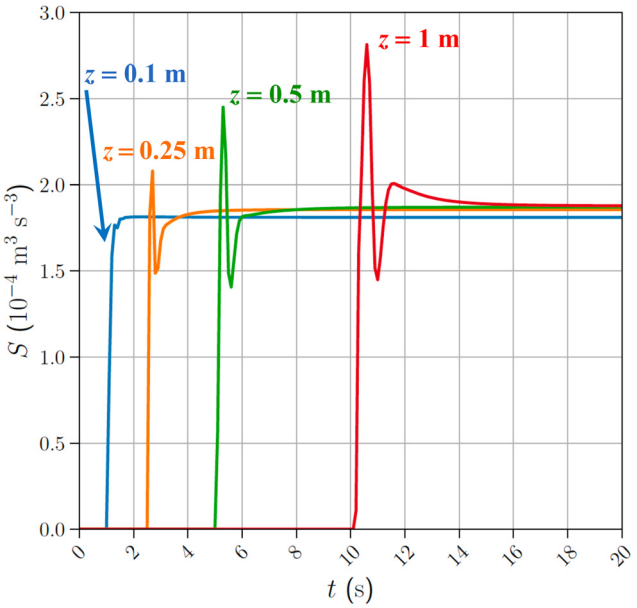

FIG. 9. Evolution of $S \equiv \sum rbw$ at selected heights.

(superscript E for exterior). Since $\mathscr{U}^E \gg \mathscr{W}^E$, the ratio of radial to vertical length scales is much less than 1: $\varepsilon^E \equiv \mathscr{L}^E/\mathscr{H}^E \sim \mathscr{W}^E/\mathscr{U}^E \ll 1$. Accordingly, the ratio of vertical to horizontal diffusion of a dependent variable ϕ, $(\partial^2\phi/\partial z^2)/(\partial^2\phi/\partial r^2) \sim (\mathscr{L}^E/\mathscr{H}^E)^2 = (\varepsilon^E)^2$, and the ratio of vertical to horizontal advection of ϕ, $(w\partial\phi/\partial z)/(u\partial\phi/\partial r) \sim (\mathscr{W}^E/\mathscr{H}^E)(\mathscr{U}^E/\mathscr{L}^E) = (\mathscr{L}^E/\mathscr{H}^E)^2 = (\varepsilon^E)^2$ are both much less than 1. We are, therefore, justified in neglecting the vertical advection and vertical diffusion terms in Eqs. (3)–(5).

An alternative scaling based on the incompressibility condition (6), in which both $\partial u/\partial r$ and u/r scale as $\mathscr{U}^E/\mathscr{L}^E$, and $\partial w/\partial z$ scales as $\mathscr{W}^E/\mathscr{H}^E$, produces $\mathscr{U}^E/\mathscr{L}^E \sim \mathscr{W}^E/\mathscr{H}^E$, which combines with $\mathscr{U}^E \gg \mathscr{W}^E$ to yield $\varepsilon^E \gg 1$. This inequality contradicts the previous result that $\varepsilon^E \ll 1$. The paradox is resolved by noting that since the magnitude of u decreases with the radius in the exterior region, $\partial u/\partial r$ and u/r have opposite signs and will at least partially cancel in their sum in Eq. (6), with total cancelation if $u \propto 1/r$ [the latter being a good approximation to u at low levels; see Fig. 5(a)]. As $|\partial u/\partial r + u/r|$ is substantially less than $|\partial u/\partial r|$ and $|u/r|$ individually, this alternative scaling is not appropriate for low-levels of the exterior region.

With their vertical advection and vertical diffusion terms neglected, Eqs. (3)–(5) become

$$u\frac{\partial u}{\partial r} = -\frac{\partial \Pi}{\partial r} + \nu\frac{\partial}{\partial r}\left[\frac{1}{r}\frac{\partial}{\partial r}(r\,u)\right], \tag{9}$$

$$u\frac{\partial w}{\partial r} = -\frac{\partial \Pi}{\partial z} + b + \frac{\nu}{r}\frac{\partial}{\partial r}\left(r\frac{\partial w}{\partial r}\right), \tag{10}$$

$$\frac{1}{r}\frac{\partial}{\partial r}(rub) = \frac{\nu}{\mathrm{Pr}}\frac{1}{r}\frac{\partial}{\partial r}\left(r\frac{\partial b}{\partial r}\right). \tag{11}$$

In arriving at Eq. (9), we have also made use of the following identity:

$$\frac{1}{r}\frac{\partial}{\partial r}\left(r\frac{\partial u}{\partial r}\right) - \frac{u}{r^2} = \frac{\partial}{\partial r}\left[\frac{1}{r}\frac{\partial}{\partial r}(r\,u)\right]. \tag{12}$$

Integration of Eq. (9) [using Eq. (8)] yields

$$\Pi = -\frac{1}{2}u^2 + \frac{\nu}{r}\frac{\partial}{\partial r}(r\,u). \tag{13}$$

Equation (11) integrates (after multiplication by r) to

$$u\,b = \frac{\nu}{\mathrm{Pr}}\frac{\partial b}{\partial r}, \tag{14}$$

where we have assumed that u and b approach their remote values (8) sufficiently rapidly, that is, $\lim_{r\to\infty} r\,b\,u = 0$ and $\lim_{r\to\infty} r\,\partial b/\partial r = 0$. Application of Eq. (13) in Eq. (10) yields

$$u\,\eta = -b + \frac{\nu}{r}\frac{\partial}{\partial r}(r\,\eta). \tag{15}$$

Eliminating u between Eqs. (14) and (15) yields

$$0 = -rb^2 + \nu\,b\frac{\partial}{\partial r}(r\,\eta) - \frac{\nu}{\mathrm{Pr}}\,r\,\eta\frac{\partial b}{\partial r}. \tag{16}$$

The identity

$$b\frac{\partial}{\partial r}(r\,\eta) - \frac{1}{\mathrm{Pr}}\,r\,\eta\frac{\partial b}{\partial r} = b^{1+1/\mathrm{Pr}}\frac{\partial}{\partial r}\left(\frac{r\,\eta}{b^{1/\mathrm{Pr}}}\right) \tag{17}$$

reduces Eq. (16) to

$$0 = -r\,b^2 + \nu\,b^{1+1/\mathrm{Pr}}\frac{\partial}{\partial r}\left(\frac{r\,\eta}{b^{1/\mathrm{Pr}}}\right). \tag{18}$$

We will return to Eq. (18) after we have approximated and partially integrated the equations governing the plume interior.

C. Steady plume interior

For the plume interior, we denote the radial and vertical velocity scales by $\mathscr{U}^I$ and $\mathscr{W}^I$ and the radial and vertical length scales by $\mathscr{L}^I$ and $\mathscr{H}^I$ (superscript I for interior). Because of the characteristic slenderness of the plume, $\varepsilon^I \equiv \mathscr{L}^I/\mathscr{H}^I \ll 1$, and we are again justified in neglecting the vertical viscous/diffusion terms in Eqs. (3)–(5). However, since the flow is mostly vertical ($\mathscr{W}^I \gg \mathscr{U}^I$), the ratio of vertical to horizontal advection of a dependent variable ϕ, $(w\partial\phi/\partial z)/(u\,\partial\phi/\partial r) \sim (\mathscr{W}^I/\mathscr{U}^I)\,\varepsilon^I$ is indeterminate. To get more information about that ratio, recall from Fig. 4 that there is a radius within the plume interior (call it R^*) at which $|u|$ attains its peak value. For $r > R^*$, $|u|$ decreases with radius, as in the plume exterior, and the incompressibility condition cannot be used to obtain a reliable scaling (see discussion in Sec. III B). However, for $r < R^*$, $\partial u/\partial r$ and u/r have the same sign, and the scaled incompressibility condition yields (legitimately) $\mathscr{W}^I/\mathscr{U}^I \sim \mathscr{H}^I/\mathscr{L}^I$. Since the ratio of vertical to horizontal advection of a variable ϕ then scales as $(w\partial\phi/\partial z)/(u\partial\phi/\partial r) \sim \mathscr{W}^I\mathscr{L}^I/(\mathscr{U}^I\mathscr{H}^I) = \mathscr{L}^I\mathscr{H}^I/(\mathscr{H}^I\mathscr{L}^I) = 1$, both vertical and horizontal advection terms should be retained. It is convenient to retain these terms over the whole interior region, not just for $r < R^*$.

With their vertical viscous/diffusion terms neglected, and Eq. (12) used to rewrite the viscous term in Eq. (3), Eqs. (3)–(5) become

$$u\frac{\partial u}{\partial r} + w\frac{\partial u}{\partial z} = -\frac{\partial \Pi}{\partial r} + \nu\frac{\partial}{\partial r}\left[\frac{1}{r}\frac{\partial}{\partial r}(ru)\right], \tag{19}$$

$$u\frac{\partial w}{\partial r} + w\frac{\partial w}{\partial z} = -\frac{\partial \Pi}{\partial z} + b + \nu\left[\frac{1}{r}\frac{\partial}{\partial r}\left(r\frac{\partial w}{\partial r}\right)\right], \tag{20}$$

$$\frac{1}{r}\frac{\partial}{\partial r}(rub) + \frac{1}{r}\frac{\partial}{\partial z}(rwb) = \frac{\nu}{\mathrm{Pr}}\left[\frac{1}{r}\frac{\partial}{\partial r}\left(r\frac{\partial b}{\partial r}\right)\right]. \tag{21}$$

It can be noted that the governing equations for the laminar plumes over point sources considered in the similarity studies of Zeldovich,[30] Yih,[32] Batchelor,[13] Fujii,[33] and Brand and Lahey[34] are consistent with our (21) (or its integrated form) and (20) (though with $\partial\Pi/\partial z$ omitted), but not (19); none of those studies made provision for a radial equation of motion.

Our analysis of Eqs. (19)–(21) is guided by the exterior plume analysis, but is more involved because of the presence of the vertical advection terms. Integration of Eq. (19) from $r = 0$ (where $u = 0$) to arbitrary r within the plume interior produces

$$\Pi = \Pi_0(z) - \int_0^r w'\frac{\partial u'}{\partial z}dr' - \left[\frac{\nu}{r}\frac{\partial}{\partial r}(ru)\right]_{r=0} - \frac{1}{2}u^2 + \frac{\nu}{r}\frac{\partial}{\partial r}(ru), \tag{22}$$

where $\Pi_0(z)$ is the centerline perturbation pressure, r' is a dummy integration variable, and other primed variables are functions of r' [e.g., $w' \equiv w(r', z)$]. To ensure continuity of Π across the plume edge, set $\Pi(R, z)$ from Eq. (22) equal to $\Pi(R, z)$ from Eq. (13), obtaining

$$\Pi_0 = \int_0^R w'\frac{\partial u'}{\partial z}dr' + \left[\frac{\nu}{r}\frac{\partial}{\partial r}(ru)\right]_{r=0}. \tag{23}$$

Application of Eq. (23) in Eq. (22) yields

$$\Pi = \int_r^R w'\frac{\partial u'}{\partial z}dr' - \frac{1}{2}u^2 + \frac{\nu}{r}\frac{\partial}{\partial r}(ru), \tag{24}$$

which, when substituted into Eq. (20), produces

$$u\eta - w\frac{\partial w}{\partial z} - \frac{\partial}{\partial z}\int_r^R w'\frac{\partial u'}{\partial z}dr' = -b + \frac{\nu}{r}\frac{\partial}{\partial r}(r\eta). \tag{25}$$

After multiplying Eq. (21) by r and integrating the result from $r = 0$ (where u and $\partial b/\partial r$ vanish) to arbitrary r ($\le R$), we get

$$ub + \frac{1}{r}\frac{\partial}{\partial z}\int_0^r r'w'b'\,dr' = \frac{\nu}{\mathrm{Pr}}\frac{\partial b}{\partial r}. \tag{26}$$

Subtracting $\eta \times$ (26) from $b \times$ (25), multiplying the result by r, and using Eq. (17) to simplify the viscous/diffusive terms yields

$$\underbrace{-rbw\frac{\partial w}{\partial z}}_{\text{Term 1}} \underbrace{-rb\frac{\partial}{\partial z}\int_r^R w'\frac{\partial u'}{\partial z}dr'}_{\text{Term 2}} \underbrace{-\frac{\partial u}{\partial z}\frac{\partial}{\partial z}\int_0^r r'w'b'dr'}_{\text{Term 3}}$$
$$\underbrace{+\frac{\partial w}{\partial r}\frac{\partial}{\partial z}\int_0^r r'w'b'dr'}_{\text{Term 4}} = \underbrace{-rb^2}_{\text{Term 5}} + \underbrace{\nu b^{1+1/\mathrm{Pr}}\frac{\partial}{\partial r}\left(\frac{r\eta}{b^{1/\mathrm{Pr}}}\right)}_{\text{Term 6}}. \tag{27}$$

We now compare the magnitudes of the terms in Eq. (27). Term 5 should be retained since it originates from the buoyancy force in Eq. (20), which drives the flow. As in the similarity studies, we assume that $w\,\partial w/\partial z \sim b$. In this case, Term 1 is of the same order of magnitude as Term 5. However, as we now show, Term 1 cancels with Term 4. Using Eqs. (A1), (A2), (A10), and (A11), we can write the sum of Term 1 and Term 4 as

$$\begin{aligned}&\text{Term 1} + \text{Term 4}\\ &= -rbw\frac{\partial w}{\partial z} + \frac{\partial w}{\partial r}\frac{\partial}{\partial z}\int_0^r r'w'b'dr'\\ &= \frac{F^2}{\nu^2 z^{1/2}}\frac{dG}{d\xi}\left[\underbrace{\frac{C}{2z}\xi^2 GH}_{\text{Term A}} + \underbrace{\frac{1}{C}\frac{\partial}{\partial z}\left(\frac{1}{z}\int_0^r r'G'H'dr'\right)}_{\text{Term B}}\right].\end{aligned} \tag{28}$$

As described in the Appendix, the vertical velocity function $G = G(\xi)$ and buoyancy function $H = H(\xi)$ are functions of the similarity variable $\xi \equiv r/R(z)$, where $R(z) = Cz^{1/2}$, $C = c\nu^{3/4}/F^{1/4}$ (c is a nondimensional number), and F is a constant representing the strength of the heat source. Using $\partial(\,)/\partial z = -[\xi/(2z)]\partial(\,)/\partial\xi$, Term B in Eq. (28) is evaluated as

$$\begin{aligned}\frac{1}{C}\frac{\partial}{\partial z}\left(\frac{1}{z}\int_0^r r'G'H'dr'\right) &= \frac{1}{C}\frac{\partial}{\partial z}\left(\frac{R^2}{z}\int_0^\xi \xi'G'H'd\xi'\right)\\ &= C\frac{\partial}{\partial z}\int_0^\xi \xi'G'H'd\xi' = -\frac{C}{2z}\xi^2 GH.\end{aligned} \tag{29}$$

As this term cancels with term A, Eq. (28) reduces to Term 1 + Term 4 = 0.

Since $\partial w/\partial r \gg \partial u/\partial z$, Term 3 is much smaller than Term 4, which is equal and opposite to Term 1, which has the same order of magnitude as Term 5. Thus, Term 3 $\ll$ Term 5 and Term 3 can be safely neglected.

Finally, we examine the ratio $T_{25} \equiv \text{Term 2}/\text{Term 5}$. Since $\partial u/\partial z \ll \partial w/\partial r$, $w\,\partial w/\partial z \sim b$, and $w|_{r=R} = 0$ [from Eq. (1)],

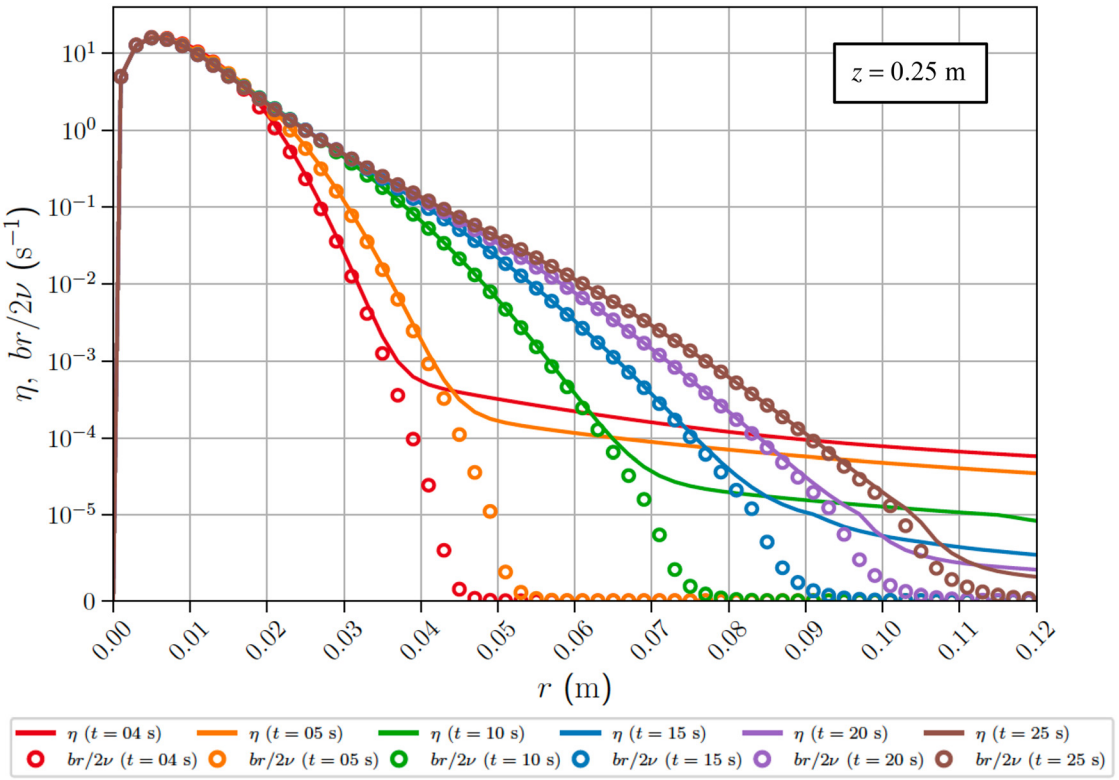

FIG. 10. Radial profiles of η (solid curves) and $br/(2\nu)$ (circles) at various times at height $z = 0.25$ m. Results are shown $t = 4$ s (shortly after plume passage) and at 5 s intervals starting at $t = 5$ s.

$$T_{25} = \frac{1}{b}\frac{\partial}{\partial z}\int_r^R w'\frac{\partial u'}{\partial z}dr' \ll \frac{1}{b}\frac{\partial}{\partial z}\int_r^R w'\frac{\partial w'}{\partial r'}dr' = \frac{1}{2b}\left(\frac{\partial w^2}{\partial z}\right)\Bigg|_r^R = -\frac{w}{b}\frac{\partial w}{\partial z} \sim 1. \tag{30}$$

Thus, $T_{25} \ll 1$, and Term 2 can be safely neglected.

With all of the terms on the left hand side of Eq. (27) canceling or being small enough to be safely neglected, Eq. (27) reduces to

$$0 = -rb^2 + \nu b^{1+1/\mathrm{Pr}}\frac{\partial}{\partial r}\left(\frac{r\eta}{b^{1/\mathrm{Pr}}}\right), \tag{31}$$

which is the same as the exterior plume relation (18).

IV. STEADY VORTICITY-BUOYANCY RELATION

Despite differences in the approximated governing equations and in locations where a radial boundary condition is imposed ($r = 0$ for plume interior, $r \to \infty$ for plume exterior), the same relation (31) [Eq. (18)] applies to both the plume interior and exterior. The results obtained in this section using that relation are, therefore, valid for any r.

A. Pr = 1

For the special case $\mathrm{Pr} = 1$, the same factor $b^{1+1/\mathrm{Pr}} = b^2$ appears in both terms of Eq. (31), and can be divided out, yielding

$$0 = -r + \nu\frac{\partial}{\partial r}\left(\frac{r\eta}{b}\right). \tag{32}$$

Integrating Eq. (32) from $r = 0$, where the vorticity vanishes but the buoyancy is non-zero, to arbitrary r, and rearranging the result yields a remarkably simple relation between the vorticity and buoyancy

$$\eta = \frac{rb}{2\nu}. \tag{33}$$

Rearranging Eq. (33) yields the inverse relation,

$$b = \frac{2\nu\eta}{r}. \tag{34}$$

The vorticity–buoyancy relation (33) [or its equivalent, (34)] is our study's main result.

We now assess the validity of Eq. (33) using buoyancy and vorticity data from the DNS. Radial profiles of η and $rb/(2\nu)$ [left and right hand sides of Eq. (33), respectively] on the $z = 0.25$ m surface are shown at different times in Fig. 10. The cap had passed through that level around $t = 3$ s (Fig. 8), which was about 1 s before the first time shown in Fig. 10. For r in the range $0\,\mathrm{m} \le r \lesssim 0.02$ m, η and $rb/(2\nu)$ are in a steady state and in good agreement with each other for all times shown. For larger radii, in the range $0.02\,\mathrm{m} \lesssim r \lesssim 0.045$ m, a steady state is reached but at progressively later times for increasing r. In this region, there is good agreement between η and $rb/(2\nu)$ in the

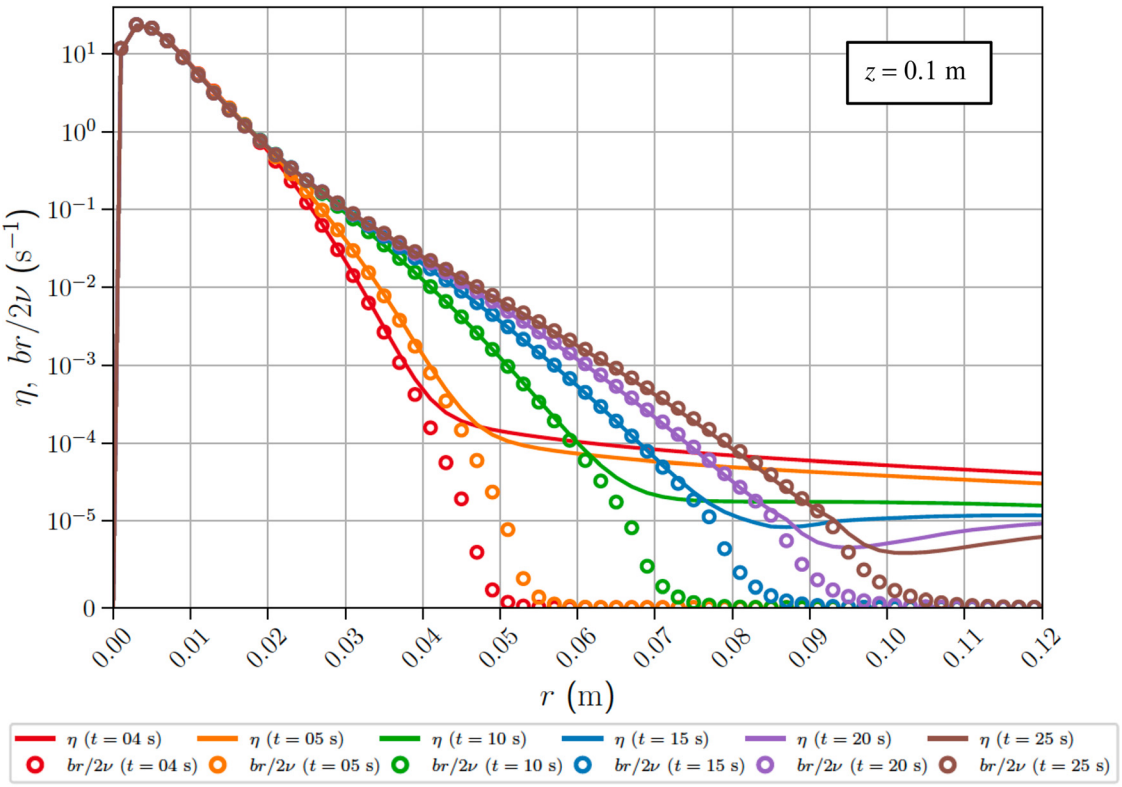

FIG. 11. As in Fig. 10, but at height $z = 0.1$ m.

steady state and also, remarkably, at earlier times, when the flow is still evolving. For $r \gtrsim 0.045$ m, a steady state is not reached by the end of the simulation but there is again good agreement between the two evolving profiles. At $t = 25$ s, η and $rb/(2\nu)$ are in good agreement for 6 orders of magnitude of their values.

Figure 11, which is analogous to Fig. 10, but for the lower elevation of $z = 0.1$ m, again shows good agreement between η and $rb/(2\nu)$. However, as seen in Fig. 3, the plume radius R at $t = 25$ s at $z = 0.1$ m is about 75% of R at $z = 0.25$ m, whether R is defined by $w = 0$ or $\partial w/\partial r = 0$. Thus, Fig. 11 shows that, at $t = 25$ s, the region over which Eq. (33) is valid extends further into the plume exterior than in Fig. 10.

It can be shown that the similarity solutions for b and w for Pr $= 1$ (e.g., Brand and Lahey[34]) with η approximated as $\eta \approx -\partial w/\partial r$, yield the same vorticity–buoyancy relation (33). However, as discussed in Secs. I and II, the similarity solution is only valid for the plume interior. The DNS confirms that the theoretical prediction (33) applies to both the plume interior and exterior and extends its validity to at least part of the transient state.

As an aside, we note that Figs. 7(a) and 10 show that in the plume interior there is a regime lasting a few seconds in which $\eta\,(\approx -\partial w/\partial r)$ is in a steady state while w is still evolving. For example, w is still evolving at $r = 0.015$ m at $t = 4$ s, at $r = 0.02$ m at $t = 5$ s, at $r = 0.03$ m at $t = 10$ s, and at $r = 0.04$ m at $t = 15$ s, while η at those same radii and times is not. We do not have an explanation for this interesting phenomenon.

B. Arbitrary Pr

A vorticity–buoyancy relation can also be derived for arbitrary Pr. Dividing (31) by $b^{1+1/\mathrm{Pr}}$ and integrating the resulting equation with respect to r yields a relation analogous to Eq. (33),

$$\eta = \frac{b^{1/\mathrm{Pr}}}{\nu r}\int_0^r r' b'^{1-1/\mathrm{Pr}} dr'. \tag{35}$$

To get the inverse relation, divide Eq. (31) by $\nu\, r\, b^2\eta/\mathrm{Pr}$, and put the result in the form of a linear equation for $1/b$,

$$\frac{\partial}{\partial r}\left(\frac{1}{b}\right) + \left(\frac{1}{b}\right)\frac{\mathrm{Pr}}{r\,\eta}\frac{\partial}{\partial r}(r\,\eta) = \frac{\mathrm{Pr}}{\nu\eta}. \tag{36}$$

It is straightforward to solve Eq. (36) using the method of integrating factors and then obtain b as

$$b = \frac{\nu}{\mathrm{Pr}}\frac{r^{\mathrm{Pr}}\eta^{\mathrm{Pr}}}{\int_0^r r'^{\mathrm{Pr}}\eta'^{\mathrm{Pr}-1}\,dr'}. \tag{37}$$

We have not explored the validity of these arbitrary-Pr expressions.

V. UNSTEADY FLOW CALCULATION, Pr = 1

We have seen that Eq. (33) applies not just to the (steady) state for which it was derived, but also to part of the evolving state following passage of the cap. To make this result plausible, we revisit the derivation of Eq. (32), with the local derivatives $\partial u/\partial t$, $\partial w/\partial t$, and $\partial b/\partial t$

included on the left hand sides of Eqs. (3)–(5), respectively, and similarly included in the equations for the plume exterior [Eqs. (9)–(11)] and interior [Eqs. (19)–(21)].

A. Unsteady plume exterior

The unsteady version of Eq. (13) is

$$\Pi = \int_r^\infty \frac{\partial u'}{\partial t} dr' - \frac{1}{2}u^2 + \frac{\nu}{r}\frac{\partial}{\partial r}(ru). \tag{38}$$

Application of Eq. (38) in the unsteady version of Eq. (10) yields

$$-\frac{\partial}{\partial t}\int_r^\infty \eta'\, dr' + u\eta = -b + \frac{\nu}{r}\frac{\partial}{\partial r}(r\eta). \tag{39}$$

The integrated thermal energy equation [analogous to Eq. (14)] is

$$-\frac{1}{r}\frac{\partial}{\partial t}\int_r^\infty b' r' dr' + ub = \nu\frac{\partial b}{\partial r}. \tag{40}$$

Subtracting $\eta \times$ (40) from $b \times$ (39), multiplying the result by r, and using Eq. (17) to simplify the viscous/diffusive terms yields

$$-rb\frac{\partial}{\partial t}\int_r^\infty \eta' dr' + \eta\frac{\partial}{\partial t}\int_r^\infty b' r' dr' = -rb^2 + \nu b^2 \frac{\partial}{\partial r}\left(\frac{r\eta}{b}\right). \tag{41}$$

If the steady vorticity-buoyancy relation (33) is applied in Eq. (41), the unsteady terms cancel, and Eq. (41) reduces to the identity $0 = 0$. In this sense, Eq. (33) is consistent with the unsteady governing equations in the exterior region.

B. Unsteady plume interior

For the plume interior, consider the unsteady form of Eq. (22),

$$\Pi = \Pi_0(z, t) - \int_0^r \frac{\partial u'}{\partial t} dr' - \int_0^r w'\frac{\partial u'}{\partial z} dr' - \left[\frac{\nu}{r}\frac{\partial}{\partial r}(ru)\right]_{r=0} - \frac{1}{2}u^2 + \frac{\nu}{r}\frac{\partial}{\partial r}(ru). \tag{42}$$

To ensure continuity of pressure across the plume edge, we set $\Pi|_{r=R}$ from Eq. (38) equal to $\Pi|_{r=R}$ from Eq. (42), obtaining

$$\Pi_0 = \int_0^\infty \frac{\partial u'}{\partial t} dr' + \int_0^R w'\frac{\partial u'}{\partial z} dr' + \left[\frac{\nu}{r}\frac{\partial}{\partial r}(ru)\right]_{r=0}, \tag{43}$$

which reduces Eq. (42) to

$$\Pi = \int_r^\infty \frac{\partial u'}{\partial t} dr' + \int_r^R w'\frac{\partial u'}{\partial z} dr' - \frac{1}{2}u^2 + \frac{\nu}{r}\frac{\partial}{\partial r}(ru). \tag{44}$$

Application of Eq. (44) in the unsteady version of Eq. (20) yields

$$-\frac{\partial}{\partial t}\int_r^\infty \eta' dr' + u\eta - w\frac{\partial w}{\partial z} - \frac{\partial}{\partial z}\int_r^R w'\frac{\partial u'}{\partial z} dr' = -b + \frac{\nu}{r}\frac{\partial}{\partial r}(r\eta). \tag{45}$$

For $\mathrm{Pr} = 1$, the unsteady version of Eq. (26) is

$$\frac{1}{r}\frac{\partial}{\partial t}\int_0^r r' b' dr' + ub + \frac{1}{r}\frac{\partial}{\partial z}\int_0^r r' w' b' dr' = \nu\frac{\partial b}{\partial r}. \tag{46}$$

Subtracting $\eta \times$ (46) from $b \times$ (45), and multiplying the result by r yields

$$-rb\frac{\partial}{\partial t}\int_r^\infty \eta' dr' + \eta\frac{\partial}{\partial t}\int_r^0 r' b' dr' + \mathrm{Term\,1} + \mathrm{Term\,2} + \mathrm{Term3} + \mathrm{Term\,4} = \mathrm{Term\,5} + \mathrm{Term\,6}, \tag{47}$$

where Term 1, …, Term 6 were defined in Eq. (27). The first term in Eq. (47) is the same as in the exterior relation (41), while the second term differs from that in Eq. (41) only in the upper limit of integration. If the steady vorticity–buoyancy relation (33) is imposed in Eq. (47), the local derivative terms combine as

$$-rb\frac{\partial}{\partial t}\int_r^\infty \eta' dr' - \eta\frac{\partial}{\partial t}\int_0^r r' b' dr' = -2\nu\eta\frac{\partial}{\partial t}\int_0^\infty \eta' dr' = -2\nu\eta\left(\frac{\partial w}{\partial t}\right)_{r=0}, \tag{48}$$

where we considered $\int_0^\infty \eta' dr'$ to be dominated by the vorticity in the plume interior and used (1): $\int_0^\infty \eta' dr' \approx \int_0^R \eta' dr' \approx -\int_0^R \partial w'/\partial r'\, dr' = -(w|_{r=R} - w|_{r=0}) = w|_{r=0}$. Recall from Figs. 7 and 8 that on any level through which the cap has passed, the centerline vertical velocity, $w|_{r=0}$, rapidly approaches its steady state; w attains a steady state first at the centerline, with a point of steadiness spreading radially outward across the plume. Thus, on any level through which the cap has passed, $\partial w/\partial t|_{r=0} \approx 0$, even though much of the plume at that level may still be evolving. In such a scenario, Eq. (33) reduces Eq. (47) to the steady state relation (27), the same arguments used in Sec. III C to justify the neglect of Term 2 and Term 3 in Eq. (27) also justify the neglect of those terms in the unsteady state, and Term 5 and Term 6 again sum to zero. However, the power laws that led to Term 1 canceling with Term 4 in the steady state may no longer apply. Indeed, an analysis of DNS data in the evolving part of the plume interior (not presented) showed that the constraint $2z\,\partial w/\partial z + r\,\partial w/\partial r = 0$, which follows from Eq. (A1), was not well satisfied. Nevertheless, with Eq. (33) imposed in Eq. (47), η approximated as $\eta \approx -\partial w/\partial r$, and $w|_{r=0}$ in a near steady state after cap passage and also relatively independent of z (recall Fig. 8), Term 1 and Term 4 do nearly cancel:

$$\begin{aligned}\mathrm{Term1} + \mathrm{Term\,4} &= -rbw\frac{\partial w}{\partial z} + \frac{\partial w}{\partial r}\frac{\partial}{\partial z}\int_0^r r' w' b' dr' \\ &\approx 2\nu\frac{\partial w}{\partial r}\left(w\frac{\partial w}{\partial z} - \frac{\partial}{\partial z}\int_0^r w'\frac{\partial w'}{\partial r'} dr'\right) \\ &= 2\nu\frac{\partial w}{\partial r}\left(w\frac{\partial w}{\partial z} - \frac{1}{2}\frac{\partial w^2}{\partial z}\Big|_0^r\right) \\ &= 2\nu\frac{\partial w}{\partial r}\left[\left(w\frac{\partial w}{\partial z}\right)\Big|_{r=0}\right] = 0.\end{aligned} \tag{49}$$

Thus, Eq. (33) has reduced the unsteady plume interior relation (47), approximately, to the identity $0 = 0$.

VI. SUMMARY AND CONCLUSIONS

We have revisited the classical problem of a steady laminar plume driven by a maintained point source of heat on a horizontal boundary. Attention is restricted to relatively weak temperature perturbations (Boussinesq dynamics), viscosity and diffusivity coefficients that are independent of temperature, and neutral stratification. Analyses of the equations of motion and thermal energy, approximated separately for the plume interior and exterior, revealed the same fundamental connection between the azimuthal vorticity and buoyancy in both regions: for a Prandtl number of 1, the vorticity is related to the buoyancy by $\eta = rb/(2\nu)$ [from Eq. (33)]. An analagous but more complex relation for arbitrary Pr was obtained as (35). A DNS of a laminar axisymmetric plume in a fluid with a Prandtl number of 1 confirmed the validity of Eq. (33) in both interior and exterior regions for the steady state (which it was derived for) and, surprisingly, also for the evolving state after cap passage. An analysis of the unsteady governing equations following the same steps used to derive (33) for the steady state made the validity of Eq. (33) plausible for unsteady flows. However, as our analysis was not a proof, the validity of Eq. (33) in unsteady conditions still needs justification.

It should be reiterated that the vorticity–buoyancy relation at the heart of our study is specific to laminar plumes over a point source of heat on a horizontal boundary. The possibility that a related or equivalent relation applies to turbulent versions of these plumes (i.e., not involving the kinematic viscosity or thermal diffusivity) was not explored.

ACKNOWLEDGMENTS

Our study has benefited from helpful discussions with Evgeni Fedorovich (University of Oklahoma).

AUTHOR DECLARATIONS

Conflict of Interest

The authors have no conflicts to disclose.

Author Contributions

Alan Shapiro: Conceptualization (lead); Formal analysis (lead); Methodology (equal); Writing – original draft (lead); Writing – review & editing (lead). **Jeremy A. Gibbs:** Data curation (lead); Formal analysis (supporting); Methodology (equal); Software (lead); Validation (lead); Visualization (lead); Writing – original draft (supporting); Writing – review & editing (supporting).

DATA AVAILABILITY

The data that support the findings of this study are available from the corresponding author upon reasonable request.

APPENDIX: POWER LAWS FOR THE PLUME INTERIOR

Using notation from Batchelor,[13] we summarize the power laws[30,32–34] for the plume interior as

$$w = \frac{F^{1/2}}{\nu^{1/2}}\, G(\xi), \tag{A1}$$

$$b = \frac{F}{\nu z}\, H(\xi), \tag{A2}$$

$$R = C z^{1/2}, \tag{A3}$$

where $\xi(r, z)$ is the nondimensional similarity variable

$$\xi \equiv \frac{r}{R(z)}. \tag{A4}$$

The positive constant F, which has dimensions of $(\text{Length})^4/(\text{Time})^3$, is proportional to the heat flux supplied by the source. The positive constant $C = c\nu^{3/4}/F^{1/4}$, where $c\,(>0)$ is a nondimensional number, has dimensions of $(\text{Length})^{1/2}$.

The power-law for u is readily obtained from Eq. (A1) and

$$u = -\frac{1}{r}\frac{\partial \psi}{\partial z}, \tag{A5}$$

$$w = \frac{1}{r}\frac{\partial \psi}{\partial r}, \tag{A6}$$

where ψ is the Stokes streamfunction.[39] In view of Eqs. (A1) and (A3), integration of $r\times$ (A6), from $r = 0$ (where ψ is a constant which, without loss of generality, is set to 0) to arbitrary r yields $\psi = (F/\nu)^{1/2}\int_0^r r' G' dr'$ or, in view of Eq. (A4),

$$\psi = \frac{C^2 F^{1/2}}{\nu^{1/2}}\, z \int_0^{\xi} \xi' G' d\xi'. \tag{A7}$$

Applying Eq. (A7) in Eq. (A5) [using $\partial\xi/\partial z = -\xi/(2z)$] then yields

$$u = \frac{C^2 F^{1/2}}{\nu^{1/2}}\frac{1}{r}\left[-\int_0^{\xi} \xi' G' d\xi' + \frac{1}{2}\,\xi^2 G\right]. \tag{A8}$$

From Eq. (A8), we obtain the shear as

$$\frac{\partial u}{\partial z} = -\frac{C F^{1/2}}{4\nu^{1/2}}\, z^{-3/2}\xi^2\,\frac{dG}{d\xi}. \tag{A9}$$

The spatial derivatives of w, obtained from Eq. (A1), are

$$\frac{\partial w}{\partial r} = \frac{F^{1/2}}{C\nu^{1/2}}\, z^{-1/2}\,\frac{dG}{d\xi}, \tag{A10}$$

$$\frac{\partial w}{\partial z} = -\frac{F^{1/2}}{2\nu^{1/2}}\, z^{-1}\,\xi\,\frac{dG}{d\xi}. \tag{A11}$$

REFERENCES

[1] J. M. Wilczak and J. E. Tillman, "The three-dimensional structure of convection in the atmospheric surface layer," J. Atmos. Sci. **37**, 2424–2443 (1980).
[2] R. B. Stull, *An Introduction to Boundary-Layer Meteorology* (Kluwer Academic Publishers, 1988), p. 670.
[3] A. G. Williams and J. M. Hacker, "The composite shape and structure of coherent eddies in the convective boundary layer," Boundary Layer Meteorol. **61**, 213–245 (1992).
[4] K. A. Emanuel, *Atmospheric Convection* (Oxford University Press, 1988), p. 592.
[5] W. Morgan, "Convective plumes in the lower mantle," Nature **230**, 42–43 (1971).
[6] R. W. Griffiths and I. H. Campbell, "Stirring and structure in mantle starting plumes," Earth Planet. Sci. Lett. **99**, 66–78 (1990).
[7] G. Schubert, D. L. Turcotte, and P. Olson, "Hot spots and mantle plumes," in *Mantle Convection in the Earth and Planets* (Cambridge University Press, 2001), pp. 499–546.

[8]I. Kumagai, A. Davaille, K. Kurita, and E. Stutzmann, "Mantle plumes: Thin, fat, successful, or failing? Constraints to explain hot spot volcanism through time and space," Geophys. Res. Lett. **35**, L16301, https://doi.org/10.1029/2008GL035079 (2008).
[9]B. Gebhart, "Buoyancy induced fluid motions characteristic of applications in technology," J. Fluids Eng. **101**, 5–28 (1979).
[10]R. C. Adhikari and M. Pahlevani, "Characteristics of thermal plume from an array of rectangular straight fins with openings on the base in natural convection," Int. J. Therm. Sci. **182**, 107798 (2022).
[11]R. Mateus, A. Pinto, and J. M. C. Pereira, "Dynamics of thermal plumes for large spaces: A comparative study of in-situ smoke test and a CFD model," Energy Build. **319**, 114512 (2024).
[12]C. Yang, Y. Jin, N. Lu, J. Xiong, S. Yu, and A. Li, "Flow characteristics of thermal plumes above rectangular heat sources with different aspect ratios," J. Build. Eng. **103**, 112043 (2025).
[13]G. K. Batchelor, "Heat convection and buoyancy effects in fluids," Q. J. R. Meteorol. Soc. **80**, 339–358 (1954).
[14]C.-S. Yih, *Fluid Mechanics: A Concise Introduction to the Theory* (West River Press, 1979), p. 622.
[15]B. Gebhart, Y. Jaluria, R. L. Mahajan, and B. Sammakia, *Buoyancy-Induced Flows and Transport* (Hemisphere Publishing Corp., 1988), p. 1001.
[16]D. J. Shlien, "Some laminar thermal and plume experiments," Phys. Fluids **19**, 1089–1098 (1976).
[17]D. J. Shlien, "Relations between point sources buoyant convection phenomena," Phys. Fluids **22**, 2277–2283 (1979).
[18]D. J. Shlien and R. L. Boxman, "Temperature field measurement of an axisymmetric laminar plume," Phys. Fluids **22**, 631–634 (1979).
[19]D. J. Shlien and R. L. Boxman, "Laminar starting plume temperature field measurement," Int. J. Heat Mass Transfer **24**, 919–931 (1981).
[20]J. Tanny and D. J. Shlien, "Velocity field measurements of a laminar starting plume," Phys. Fluids **28**, 1027–1032 (1985).
[21]P. Olson and H. Singer, "Creeping plumes," J. Fluid Mech. **158**, 511–531 (1985).
[22]E. Moses, G. Zocchi, I. Procaccia, and A. Libchaber, "The dynamics and interaction of laminar thermal plumes," Europhys. Lett. **14**, 55–60 (1991).
[23]E. Moses, G. Zocchi, and A. Libchaber, "An experimental study of laminar plumes," J. Fluid Mech. **251**, 581–601 (1993).
[24]E. Kaminski and C. Jaupart, "Laminar starting plumes in high-Prandtl-number fluids," J. Fluid Mech. **478**, 287–298 (2003).
[25]J. Vatteville, P. E. van Keken, A. Limare, and A. Davaille, "Starting laminar plumes: Comparison of laboratory and numerical modeling," Geochem. Geophys. Geosyst. **10**, Q12013 (2009).
[26]M. C. Rogers and S. W. Morris, "Natural versus forced convection in laminar starting plumes," Phys. Fluids **21**, 083601 (2009).
[27]A. Davaille, A. Limare, F. Touitou, I. Kumagai, and J. Vatteville, "Anatomy of a laminar starting thermal plume at high Prandtl number," Exp. Fluids **50**, 285–300 (2011).
[28]N. Cagney, W. H. Newsome, C. Lithgow-Bertelloni, A. Cotel, S. R. Hart, and J. A. Whitehead, "Temperature and velocity measurements of a rising thermal plume," Geochem. Geophys. Geosyst. **16**, 579–599 (2015).
[29]P.-J. Qin, Y.-Y. Hou, J.-D. He, P. Wei, and S.-D. Huang, "Formation and evolution of laminar thermal structures: Correlation to the thermal boundary layer and effects of heating time," J. Fluid Mech. **984**, A60 (2024).
[30]Y. B. Zeldovich, "The asymptotic laws of freely-ascending convective flows," Zh. Eksper. Teor. Fiz. **7**, 1463–1465 (1937).
[31]*Selected Works of Yakov Borisovich Zeldovich*, Chemical Physics and Hydrodynamics Vol. 1, edited J. P. Ostriker, G. I. Barenblatt, and R. A. Sunyaev (Princeton University Press, 1992), pp. 82–85.
[32]C.-S. Yih, "Free convection due to a point source of heat," in *Proceedings of the First U.S. National Congress of Applied Mechanics* (ASME, New York, 1951), pp. 941–947.
[33]T. Fujii, "Theory of the steady laminar natural convection above a horizontal line heat source and a point heat source," Int. J. Heat Mass Transfer **6**, 597–606 (1963).
[34]R. S. Brand and F. J. Lahey, "The heated laminar vertical jet," J. Fluid Mech. **29**, 305–315 (1967).
[35]H. Schlichting, *Boundary-Layer Theory*, 7th ed. (McGraw-Hill, 1979), p. 817.
[36]C. C. van Heerwaarden, B. J. H. van Stratum, T. Heus, J. A. Gibbs, E. Fedorovich, and J. P. Mellado, "MicroHH 1.0: A computational fluid dynamics code for direct numerical simulation and large-eddy simulation of atmospheric boundary layer flows," Geosci. Model Dev. **10**, 3145–3165 (2017).
[37]G. I. Taylor, "Flow induced by jets," J. Aerosp. Sci. **25**, 464–465 (1958).
[38]K. Kraemer, "Die Potentialströmung in der Umgebung von Freistrahlen," Z. Flugwiss **19**, 93–104 (1971).
[39]P. K. Kundu and I. M. Cohen, *Fluid Mechanics*, 2nd ed. (Academic Press, 2002), p. 730.